Chapter 6

Weakly nonlinear analysis

Never I encountered a problem which did not become more complicated on careful examination

P. Anderson

The linear analysis of the WEM presented in the previous chapter predicts a threshold shift with respect to the SM and, for sufficiently low recombination rates, a Hopf bifurcation to travelling rolls. Further questions can be treated at the weakly-nonlinear level. Is the bifurcation continuous (forward) or hysteretic (backward)? If it is forward, which combinations of degenerate linear modes will be selected by the dynamics? For instances, for a Hopf bifurcation, the dynamics can select travelling waves or standing waves, i.e., a superposition of left and right travelling waves. In the oblique-roll regime, isolated regions of "zig" or "zag" modes, or a superposition of both, can be favoured; for travelling oblique waves there are even more possibilities. Furthermore, how does the frequency of the travelling waves depend on the reduced control parameter $\epsilon = R/R_c - 1$? Finally, can the observation of chaos at onset [30, 31] be explained within the framework of the weakly-nonlinear analysis?

If the bifurcation is hysteretic, there is the question of the amplitude and of the type (e.g., stationary or oscillatory) of the nonlinear final state, and of the range of the control parameters where hysteresis effects take place. Upon decreasing the control parameter, when does the system jump back to the unstructured state?

The basic idea of the weakly-nonlinear analysis [1, 102, 103] is to reduce the phase space of the system to that of the slowly relaxing "dynamically active" modes. The remaining fast degrees of freedom are "slaved" [1] to these modes. This idea uses the fact that, if one starts with general initial conditions (with a general point in the phase space of the system), the state in phase space will approach on a fast time scale the subspace spanned by the slowly relaxing degrees of freedom, and the

subsequent dynamics will take place on this subspace. For recent reviews see, e.g., [9, 50, 24] or [104].

The (still infinitely dimensional) set of these dynamically active degrees of freedom can be constructed from modes on the same dispersion branches as the critical modes, with wave vectors close to the critical wave vectors. In addition, this set may contain slowly relaxing modes generated by the nonlinearities.

In Chapter 6.1, I discuss the Ginzburg–Landau approach and give the (uncoupled) complex Ginzburg–Landau equation (CGL) for the WEM in the special case of a one-dimensional dynamics of left-travelling waves (LTW) (or, equivalently, right-travelling waves).

Chapter 6.2 gives analytic expressions for the coefficients of this CGL. Rather than providing quantitative numerical results, the goal is a qualitative (at most semi-quantitative) understanding of the nonlinear behaviour of the WEM. In particular, the intricate influence of the WEM mobility parameter $\tilde{\alpha}$ and the recombination parameter $\tilde{r}$ on the dynamics will be elucidated by means of analytic expressions containing explicitely these parameters.

In Chapter 6.3, I summarize the weakly-nonlinear results of the WEM by phase diagrams in the WEM parameter space $(\tilde{\alpha}, \tilde{r})$ and by an expression for the change of the oscillation frequency with the control parameter in the Hopf regime. The predictions are compared with experiments on MBBA and I 52. Furthermore, I give estimates for the nonlinear amplitude in the stationary-hysteretic regime assuming no WEM effects in the nonlinear state. Most results agree, within factors of about two with the experiments.

Chapter 6.4 gives a discussion of the weakly-nonlinear results.

6.1 Ginzburg-Landau equations for the WEM

With at most discrete degeneration of the critical mode, the near-threshold dynamics can be described, for a continuous bifurcation, by a set of third-order coupled Ginzburg–Landau equations (CCGL) for the envelopes (or amplitudes) $A_m(x, y, t)$ of wave packets with wave vectors near that of the mth mode in the set of the degenerated critical modes. For oblique travelling rolls, this involves a total of four amplitudes for the modes of the right and left-travelling "zig" and "zag" rolls. For a hysteretic bifurcation, one needs at least fifth-order CCGLs with a stabilizing fifth-order term to counteract the destabilizing third-order contribution.

For simplicity, I restrict the treatment to one lateral dimension, x, and to modes near the critical mode $\propto e^{i(\mathbf{q}\cdot\mathbf{x}+\omega t)}$ for left-travelling waves (LTW) leading to a one-

dimensional uncoupled CGL. Some relevant experimental results (especially those for I 52 [30, 31]) are for the regime of oblique rolls and the weakly-nonlinear description for, say, the wave packet of the LTWs with $p_c > 0$, would require a two-dimensional CGL. Nevertheless, one can expect that, like q_c and ω_H in the linear regime, many weakly-nonlinear aspects of the oblique-roll regime can be described, at least semi-quantitatively, by dropping the y dependence. [1]

Restricting to left-travelling rolls (and to $p > 0$ for oblique rolls), the set of slowly-relaxing modes can be represented as a wave packet with wave vectors around that of the critical LTW,

$$\begin{aligned} \boldsymbol{u} &= \boldsymbol{u}^{(1)} + \text{higher order terms}, \\ \boldsymbol{u}^{(1)} &= A(\boldsymbol{x},t)\tilde{\boldsymbol{u}}(z,\omega_0 t)e^{i[\mathbf{q}_c\cdot\mathbf{x}+\omega(\mathbf{q}_c,\epsilon)t]} + \text{c.c.} \end{aligned} \tag{6.1}$$

The complex amplitude $A(\boldsymbol{x},t)$ varies slowly in x, y and in time but the y dependence will be dropped. The spatial variation $e^{i\mathbf{q}_c\cdot\mathbf{x}}$ of the critical mode and its frequency (the imaginary part of the linear growth rate) at $\boldsymbol{q} = \boldsymbol{q}_c$ and at the *actual* value of the control parameter is separated out. The function $\tilde{\boldsymbol{u}}$ is the Floquet function, Eq. (5.14), for the LTW at threshold and contains the z dependence and the periodicity with the external field. Within the lowest-order Floquet and Galerkin expansions, $\tilde{\boldsymbol{u}}$ is given by Eq. (5.15) where $(\sigma^{(0)}, \phi^+, \phi^-, n_z^{(0)}, \cdots)$ is the eigenvector composed of the Galerkin coefficients, given by Eq. (5.17) for $\boldsymbol{q} = \boldsymbol{q}_c$, $R = R_c$, and $\lambda = i\omega_H$. For quantitative statements about nonlinear (or stochastic) properties, the normalization of the eigenfunctions is important. It is chosen such that $|A|$ gives directly the maximum director angle $\arctan(n_z) \approx n_z$ at $z = 0$, which can be measured directly by the shadowgraph method [105],

$$n_z(\boldsymbol{r},t) = |A(x,t)| \cos z \cos[\boldsymbol{q}_c \cdot \boldsymbol{x} + \omega(\epsilon,\boldsymbol{q}_c)t + \phi_A] \tag{6.2}$$

with $\phi_A = \arg(A)$. For the coefficients of the one-mode expansion (5.15), this corresponds to $n_z^{(0)} = (2\pi)^{1/2}$.

The form of the amplitude equation is determined completely by symmetry constraints [9],

$$\tau_0(\partial_t - v_g\partial_x)A = [\epsilon + \xi_0^2(1+ib)\partial_x^2]A - g(1+ic)|A|^2 A. \tag{6.3}$$

There are several ways to derive the coefficients. These include the introduction of multiple scales and a subsequent systematic expansion, or the use of "order-parameter equations in $\boldsymbol{q}$ space together with projection techniques employing the "slaving principle" [1].

[1] The nonlinear selection of the zig and zag modes, of course, cannot be described by this approximation.

The multiscale approach was first applied to RBC in simple fluids [102]. Other systems include, e.g., lasers [106] or EHC [48]. For reviews see, e.g., [104, 24, 10].

The order-parameter approach has been applied, e.g., for thermal convection in simple fluids [103], thermal convection in homeotropically aligned EHC, [107, 108], and to EHC [50].

It turns out that the linear coefficients are obtained most easily by using the projection method which, in this case, reduces to an expansion of the growth rate around the threshold (Chapter 6.2.1). The nonlinear coefficients g and c can be calculated easier with the multiple-scale method (Chapter 6.2.2).

6.2 Coefficients of the one-dimensional complex Ginzburg-Landau equation

In addition to the asumptions made in Chapter 5 (adiabatic elimination of the charge and the velocities, lowest-order Galerkin and Floquet expansions), I consider external frequencies satisfying (in physical units) $\omega_0\tau_q << 1$ and $\omega_0\tau_d >> 1$.

The decisive new nonlinearity of the WEM is the term $\boldsymbol{v}\cdot\boldsymbol{\nabla}\sigma$ associated with advection of the carrier density, Eq. (3.28). It can be argued that the saturation of the $\pm q_c$ modes of all SM fields is not altered by WEM effects. Furthermore, I neglect the interaction of the σ modes with intermediate modes excited by second-order SM nonlinearities. This last assumption (whose validity has yet to be investigated) allows an adiabatic elimination of ρ and $\boldsymbol{v}$ also for the nonlinear case by generalizing the effective quantities in Eq. (5.38) to allow for an amplitude dependence. [2]

With these assumptions, the Eqs. (3.28) and (3.29) can be written as

$$\begin{aligned}\left(\partial_t-\hat{\lambda}_\sigma\right)\sigma-R\check{\alpha}^2\hat{\sigma}_a^{(\mathrm{eff})}\,\partial_x\partial_z n_z &= -(\boldsymbol{v}\cdot\boldsymbol{\nabla})\sigma \\ &- R\check{\alpha}^2\hat{\sigma}_a^{(\mathrm{eff})}\,g^{\mathrm{SM}}|A(x,t)|^2\partial_x\partial_z n_z, \qquad (6.4)\\ -\frac{R\hat{C}^2}{\hat{\sigma}_a^{(\mathrm{eff})}}\partial_z\sigma+\left(\partial_t-\hat{\lambda}_n\right)\partial_x n_z &= -g^{\mathrm{SM}}|A(x,t)|^2\left(\frac{\partial_x n_z}{\tau_0^{\mathrm{SM}}}+\frac{R\hat{C}^2}{\hat{\sigma}_a^{(\mathrm{eff})}}\partial_z\sigma\right), \qquad (6.5)\end{aligned}$$

where $g^{\mathrm{SM}} = 0.48$ for MBBA at $\omega_0\tau_q << 1$ and for the normalization (6.2) [48]. The left-hand sides contain the linear terms; the quantities $\hat{\lambda}_\sigma$, $\hat{\sigma}_a^{(\mathrm{eff})}$, $\hat{C}$, and $\hat{\lambda}_n$ are operators which reduce to the corresponding effective quantities λ_σ, $\sigma_a^{(\mathrm{eff})}$, C and λ_n

[2] This is a standard method in nonlinear optics. If, e.g., in laser-active dielectric materials, the time scales of the polarization and inversion fields are much shorter than that of the optical field $\boldsymbol{E}$, one can introduce an effective dielectric permittivity which is $\propto(1+g|\boldsymbol{E}|^2)^{-1}$ [106].

Table 6.1: Linear coefficients of the Ginzburg Landau equation in the approximation $R\tilde{\alpha}^2 << 1$

Quantity	Hopf range	Stationary range
τ_0	$2\left(\frac{1}{\tau_0^{\rm SM}} - \frac{R\tilde{\alpha}^2\epsilon_q}{\sigma_q(1+\omega'^2)}\right)^{-1} \approx 2\tau_0^{\rm SM}$ *	$\tau_0^{\rm SM}\frac{\left(1-\frac{\tilde{\omega}^2}{\lambda_\sigma^2}\right)}{1+2\tau_0^{\rm SM}\frac{\tilde{\omega}^2}{\lambda_\sigma}}$
ξ_0^2	$\xi_{0,\rm SM}^2$	$\xi_{0,\rm SM}^2 - \frac{(\tau_0^{\rm SM})^3\tilde{\omega}^4}{\tau_0^2\lambda_\sigma^3}\left(\frac{\partial_q C^2}{C^2}\right)^2$ †
b	$\frac{\lambda_\sigma}{\omega_H} + \frac{\tau_0^{\rm SM}}{\xi_{0,\rm SM}^2\omega_H}\left(v_g^2 - \partial_q(\tilde{\omega}\partial_q\tilde{\omega})\right)$ **	$--$
v_g	$\frac{\tilde{\omega}\partial_q\tilde{\omega}}{\omega_H}$ **	$--$
$\frac{\partial\omega}{\partial\epsilon}$	$\frac{\tilde{\omega}^2}{\omega_H} + \frac{\lambda_\sigma}{2\tau_0^{\rm SM}\omega_H}$	$--$

*The first expression is without the approximation $R\tilde{\alpha}^2 << 1$
†Approximation $\tilde{\omega} << 1/\tau_0^{\rm SM}$
**Approximation $R\tilde{\alpha}^2 << \tilde{\omega}$

of Chapter 5, if applied to the SM modes. For other modes, they are understood as numbers resulting from the Galerkin approximations for the actual modes (see below). For the Galerkin approximation (5.39) and (5.40) of critical modes, the left-hand side reduces to Eq. (5.38).

The nonlinear terms are on the right-hand sides. The only second-order nonlinearity is the advection term $-\boldsymbol{v}\cdot\boldsymbol{\nabla}\sigma$ in Eq. (6.4). The term $\propto \partial_x n_z$ in Eq. (6.5) is the saturating SM nonlinearity. The other two terms $\propto R$ describe the saturation of the coupling from the σ to the n_z mode, and *vice versa*. The coupling is mediated by the charge density and it can be shown [109], that the saturation of the SM mode is primarily due to the nonlinearities in the charge focussing effect of the director bend. So I assume that this coupling saturates like the SM mode.

6.2.1 Linear coefficients

The linear coefficients of the CGL (6.3) can be obtained directly by the projection method. With the ansatz $\overline{\boldsymbol{u}} = \bar{A}_{\mathbf{q}-\mathbf{q}_c}(t)\tilde{\boldsymbol{u}}e^{i\omega(\mathbf{q}_c,\epsilon)t}$, the eigenvalue problem for the growth rate of the critical branch can be written as

$$\partial_t \bar{A}_{\mathbf{k}} = \left[\lambda(\boldsymbol{q}_c + \boldsymbol{k},\epsilon) - i\omega(\boldsymbol{q}_c,\epsilon)\right]\bar{A}_{\mathbf{k}}, \tag{6.6}$$

where $\boldsymbol{k} = \boldsymbol{q} - \boldsymbol{q}_c$. Taking, in lowest order, the Floquet function $\tilde{\boldsymbol{u}}$ at $\boldsymbol{q} = \boldsymbol{q}_c$, an inverse Fourier transformation of the ansatz back to real space results in Eq. (6.1) with

$$\partial_t A(\boldsymbol{x}, t) = [\lambda(\boldsymbol{q}_c - i\boldsymbol{\nabla}, \epsilon) - i\omega(\boldsymbol{q}_c, \epsilon)]\, A(\boldsymbol{x}, t). \tag{6.7}$$

The linear coefficients of the one-dimensional CGL are obtained in terms of the linear growth rate by comparing Eq. (6.3) with the Taylor expansion of Eq. (6.7) with respect to $q_c - i\partial_x$ and ϵ around $\boldsymbol{q} = \boldsymbol{q}_c$ and $\epsilon = 0$. The result is $\tau_0^{-1} = \partial_\epsilon \sigma|_c$, $v_g = \partial_q \omega|_c$, and $\xi_0^2(1 + ib) = -\frac{\tau_0}{2}\partial_q^2 \lambda|_c$, where $\lambda = \sigma + i\omega$ and $|_c$ stands for the critical point $\boldsymbol{q} = \boldsymbol{q}_c$ and $\epsilon = 0$. In addition, one obtains the linear frequency shift, $\Delta\omega := \omega(\boldsymbol{q}_c, \epsilon) - \omega_H = \epsilon \partial_\epsilon \omega|_c$.

Table 6.1 gives approximate analytic expressions for these coefficients using Eq. (5.47) for the growth rate, both for the Hopf regime $\tilde{\omega} > |\lambda_\sigma|$, and for the stationary regime $\tilde{\omega} < |\lambda_\sigma|$, separated by the codimension-two (C2) curve.

The Figures 6.1 and 6.2 show the real and imaginary CGL coefficients for I 52 parameters. Remarkably, the correlation time τ_0 in the Hopf regime is nearly twice the time in both the SM and in the stationary regime not too near to the C2 curve. This can be seen directly from the real part of the growth rate (5.47) which is $\sigma = (\lambda_\sigma + \lambda_n)/2$ in the Hopf regime, while it is $\sigma \approx \lambda_n$ in the stationary regime far away from the C2 curve. For most situations, the ϵ dependence $\propto \tilde{\alpha}^2$ of λ_σ, Eq. (5.41), is negligible compared to that of λ_n. This leads to the factor of 2 in $\tau_0 = (\partial_\epsilon \sigma)^{-1}$.

The correlation time goes to zero and the correlation length diverges if one approaches the C2 curve from the stationary side (Figures 6.1a and 6.1b). This is caused by the dependence of the square root in Eq. (5.47) on, respectively, ϵ and $\boldsymbol{q}$, together with the divergence of the gradient of the square root at the C2 point. Approaching the C2 point from the Hopf region, the diverging gradient leads to vanishing factors of ω_H in the denominators of the expressins for $\frac{\partial \omega}{\partial \epsilon}$, v_g, and b, causing the singularities of these quantities at the C2 point

If the Hopf condition is well satisfied and $\omega_0 \tau_q << 1$, the group velocity $v_g \approx R_c \tilde{\alpha} \frac{\partial C}{\partial q}|_c$ has the same sign as the phase velocity ω_H / q_c of the critical mode; the ratio $v_g/(\omega_H/q_c) = C^{-1}\frac{\partial C}{\partial q}|_c$, is slightly smaller than 1, both for MBBA and I 52 (Fig. 5.5). For most parameters, the expression for the dispersion coefficient b is mainly determined by the negative relaxation term $\lambda_\sigma/\tilde{\omega}$. For very small recombination rates or very high mobility parameters, the term $\propto \partial_q(\tilde{\omega}\partial_q\tilde{\omega})$ becomes important; it is essentially proportional to the negative curvature of $C(q)$, i.e., positive for both MBBA and I 52 (Fig. 5.5). The divergence of b at the C2 point is due to the v_g^2 term.

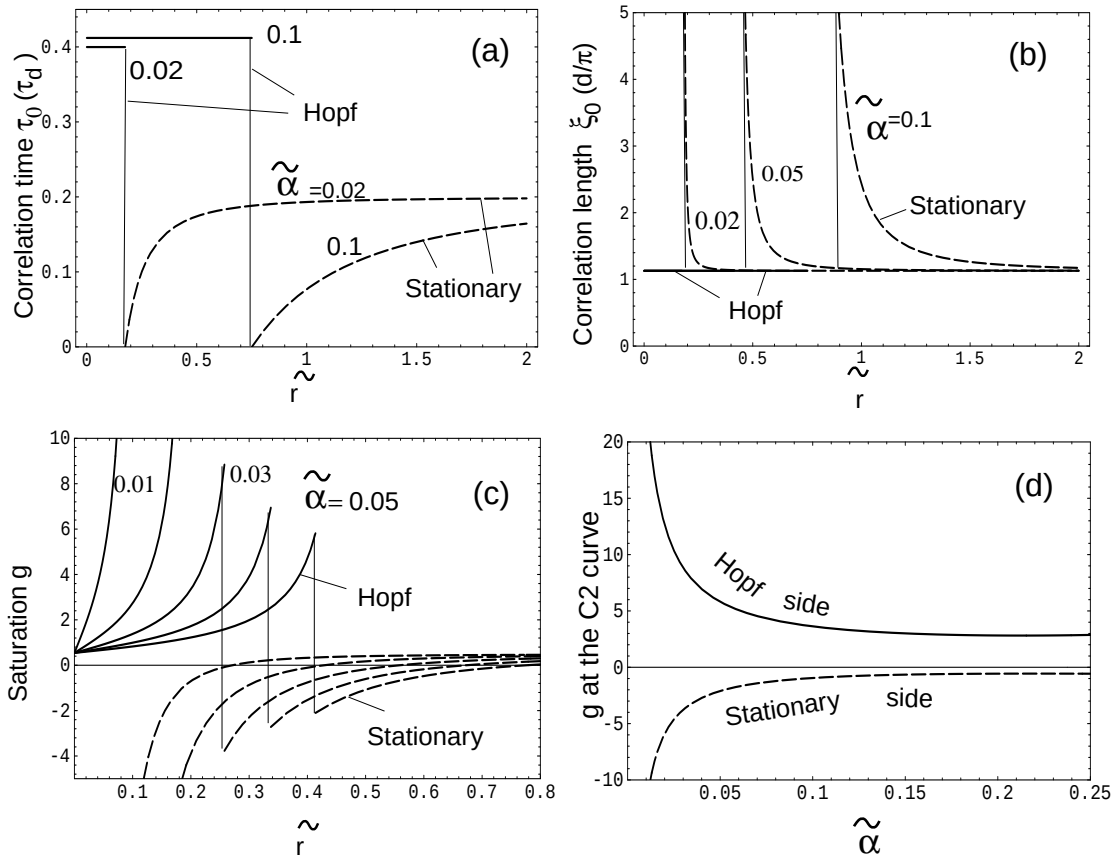

Figure 6.1 (a)-(c) plots of the real Ginzburg–Landau coefficients τ_0 and ξ_0^2 (Table 6.1), and g (Table 6.2) for I 52 at 45°C and for $\omega_0\tau_q << 1$. The full lines are for the Hopf regime of travelling waves and the dashed lines for the stationary regime. Parameter is the mobility parameter $\tilde{\alpha}$, where $\tilde{\alpha} = 0.01 \cdots 0.04$ is the order of magnitude in the MBBA and I 52 experiments, and $\tilde{\alpha} = 0.1$ corresponds to very thin cells.
(d) Nonlinear saturation g along the C2 curve approaching the C2 curve from the Hopf regime (full line) and from the stationary regime (dashed). Several approximations have been applied in calculating the nonlinear coefficients, see the main text.

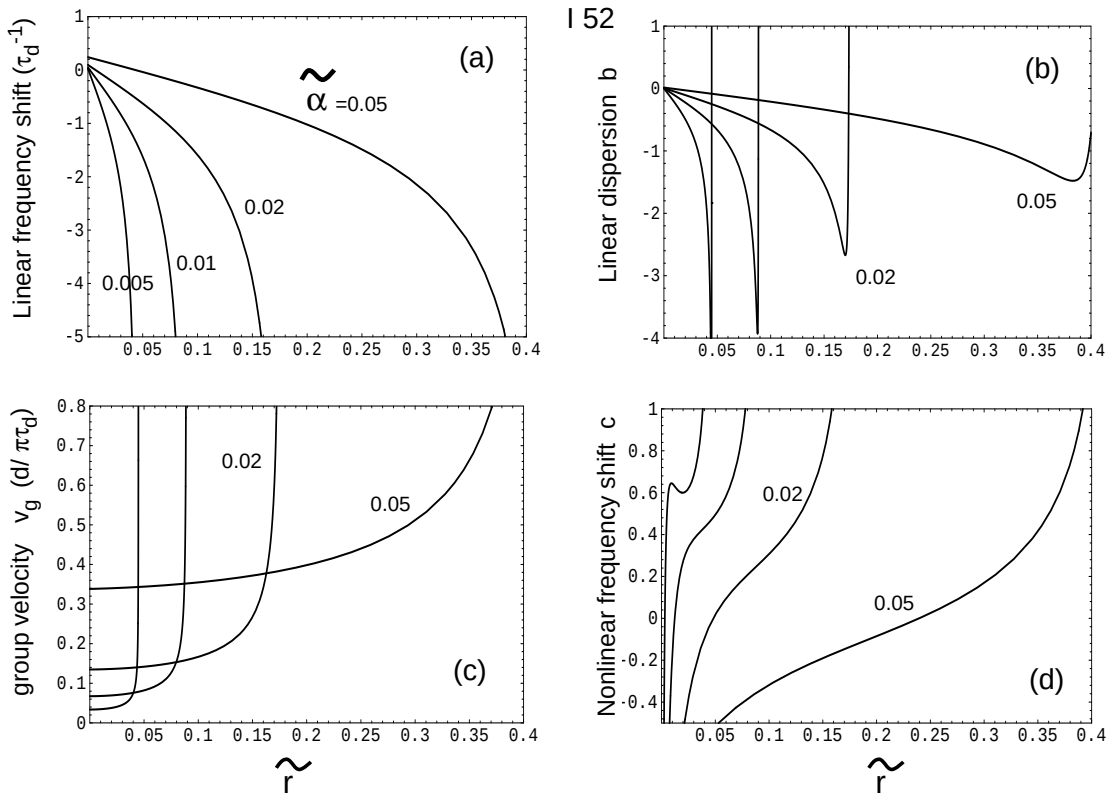

Figure 6.2 (a) linear frequency shift; (c) group velocity, and (b), (d), the imaginary parameters of the CGL in the Hopf regime for I 52 at 45°C and for external frequencies satisfying $\omega_0\tau_q << 1$. The linear dispersion b is proportional to $\frac{\partial^2\omega}{\partial q^2}$, and the nonlinear frequency shift c is proportional to $-\frac{\partial\omega}{\partial|A|^2}$.

At last, the linear frequency shift is negative, apart from the case of very small recombination rates or high values of $\tilde{\alpha}$, where the positive term $\propto \tilde{\omega}^2/\omega_H$ becomes the main contribution. This term reflects the dependence of the coupling $\tilde{\omega} = R\tilde{\alpha}C$ on R.

6.2.2 Nonlinear coefficients

Now I derive the saturation coefficient g and the nonlinear frequency shift c of the CGL (6.3) by a systematic multiple-scale expansion. In this method (a pedagogical example can be found in Ref. [10]), one starts with the ansatz

$$\boldsymbol{u} = \boldsymbol{u}^{(1)} + \boldsymbol{u}^{(2)} + \boldsymbol{u}^{(3)} + \cdots, \tag{6.8}$$

where $\boldsymbol{u}^{(1)}$ is given by Eq. (6.1) in terms of the amplitude, and $\boldsymbol{u}^{(i)}$ is of the order of $|A(x,t)|^i$. Inserting this ansatz into the nonlinear basic equations assuming

$$\mathcal{O}(\partial_t - v_g\partial_x) = \mathcal{O}(\partial_x^2) = \mathcal{O}(|A|^2) = \mathcal{O}(\epsilon) \tag{6.9}$$

for all derivatives acting onto A, and separating into orders of $\epsilon, \epsilon^{3/2}, \cdots$ leads to a hierarchy of linear inhomogeneous equations of the form $\underline{\underline{\tilde{L}}}\boldsymbol{u}^{(i)} = I^{(i)}$. The operator $\underline{\underline{\tilde{L}}}$ contains all linear parts of the basic equations; the inhomogenities $I^{(i)}$ are given in terms of $\boldsymbol{u}^{(i-1)} \cdots \boldsymbol{u}^{(1)}$, calculated already in terms of A and $\tilde{\boldsymbol{u}}$ in the previous steps.

These inhomogeneous equations can be solved nontrivially only, if the $I^{(i)}$ are not in the kernel (null space) of $\underline{\underline{\tilde{L}}}^\dagger$, the operator adjoint to $\underline{\underline{\tilde{L}}}$ (Fredholm alternative). These "compatibility conditions" determine the amplitude equation to the desired order.

Now I apply this method to the "basic equations" (6.4) and (6.5). The solvability condition at $\mathcal{O}(\epsilon)$ leads to $\partial_t A - \frac{\partial\omega}{\partial q}|_c \partial_x A + \mathcal{O}(\epsilon^{3/2}) = 0$ defining $v_g = \frac{\partial\omega}{\partial q}|_c$. [3] This result has been obtained already more directly by the projection technique and will not be shown explicitely here. [4] The solvability condition at the next order $\epsilon^{3/2}$ determines the remaining coefficients of the CGL (6.3).

Since I am interested only in the nonlinear parts $\propto |A|^2 A$ which are already of order $\epsilon^{3/2}$, I neglect all derivatives acting on A ("exact resonance") and show the systematic expansion by starting, instead of Eq. (6.1), with the zero-dimensional ansatz[5]

$$\boldsymbol{u}^{(1)} = A(t)\tilde{\boldsymbol{u}}(z,\omega_0 t)e^{i(\mathbf{q}_c\cdot\mathbf{x}+\omega_H t)} + \text{c.c.}, \tag{6.10}$$

$$\tilde{\boldsymbol{u}}(z,\omega_0 t) \equiv \begin{pmatrix} \tilde{\sigma} \\ \tilde{n}_z \end{pmatrix} = \frac{1}{2}\begin{pmatrix} \sigma^{(0)}\sin z \\ \cos z \end{pmatrix}; \quad \sigma^{(0)} = \left.\frac{iq_c R_c \tilde{\alpha}^2 \sigma_a^{(\text{eff})}}{\lambda_\sigma - i\omega_H}\right|_c. \tag{6.11}$$

[3] In stationary pattern-forming systems like RBC or the SM of EHC, the solvability condition at this order is, usually, fulfilled automatically.

[4] An example of a nontrivial solvability condition at this order is given, e.g., in Ref. [106].

[5] This is the usual way to derive normal forms for low-dimensional systems ("Landau equations")

The inhomogeneous equations at order ϵ read

$$\left(\partial_t - \hat{\lambda}_\sigma\right)\sigma^{(2)} \quad -R\tilde{\alpha}^2\hat{\sigma}_a^{(\mathrm{eff})}\,\partial_x\partial_z n_z^{(2)} \quad = -\boldsymbol{v}^{(1)}\cdot\boldsymbol{\nabla}\sigma^{(1)}, \tag{6.12}$$

$$-\frac{R\hat{C}^2}{\hat{\sigma}_a^{(\mathrm{eff})}}\partial_z\sigma^{(2)} \quad +\left(\partial_t - \hat{\lambda}_n\right)\partial_x n_z^{(2)} \quad = 0. \tag{6.13}$$

For the Hopf regime, the second-order inhomogeneity is

$$\begin{aligned}\boldsymbol{v}^{(1)}\cdot\boldsymbol{\nabla}\sigma^{(1)} &= \frac{\pi(K^{(\mathrm{eff})})^2\eta^{(\mathrm{eff})}\,\tilde{\alpha}^2}{8\tilde{\omega}^2}\Big\{(\lambda_\sigma + i\omega_H)A^2e^{2i(\mathbf{q}_c\cdot\mathbf{x}-\omega_H t)}f_1(z) + \text{c.c.}\\ &- 2\sqrt{\frac{2}{\pi}}\lambda_\sigma|A|^2\partial_z\left[C_1(z)\sin z\right]\Big\}.\end{aligned} \tag{6.14}$$

The inhomogeneity for a stationary bifurcation is obtained by the substitutions $\tilde{\omega}^2 \to \lambda_\sigma^2$, and $\omega_H \to 0$. The function $f_1(z) = (2/\pi)^{1/2}[C_1(z)\cos z - \sin z\partial_z C_1(z)]$ has strong variations only near the boundaries (it would be equal to 1 for free BC).

This inhomogeneity does not lie in the kernel of the adjoint linear operator and drives the second-order charge-carrier modes. Solving Eqs. (6.12) and (6.13) with the BCs $\partial_z\sigma^{(2)} = n_z^{(2)} = 0$ for quasi-stationary conditions (i.e., the dynamics of the excited modes is fast compared to that of A), results, in the lowest-order Galerkin approximation, in two types of modes,

$$\begin{aligned}\boldsymbol{u}^{(2)} = \boldsymbol{u}_0^{(2)} + \boldsymbol{u}_2^{(2)} &= C_0^{(2)}\begin{pmatrix}\sqrt{\frac{2}{\pi}}\cos 2z\\ 0\end{pmatrix}|A|^2\\ &+ C_2^{(2)}\begin{pmatrix}\sqrt{\frac{1}{\pi}}\\ 0\end{pmatrix}A^2e^{2i(\mathbf{q}_c\cdot\mathbf{x}+\omega_H t)} + \text{c.c.},\end{aligned} \tag{6.15}$$

with the amplitudes

$$C_0^{(2)} = -\frac{\pi I_0(K^{(\mathrm{eff})})^2\eta^{(\mathrm{eff})}\,\tilde{\alpha}^2\lambda_\sigma}{4\tilde{\omega}^2\lambda_0^{(2)}}, \tag{6.16}$$

$$C_2^{(2)} = \frac{\pi I_2(K^{(\mathrm{eff})})^2\eta^{(\mathrm{eff})}\,\tilde{\alpha}^2(\lambda_\sigma + i\omega_H)}{2\sqrt{2}\tilde{\omega}^2\lambda_2^{(2)}}, \tag{6.17}$$

the growth rates

$$\lambda_0^{(2)} = -(\tilde{r} + 4R_c\tilde{\alpha}^2), \quad \lambda_2^{(2)} = -(\tilde{r} + 2i\omega_H), \tag{6.18}$$

and the projection integrals

$$I_0 = \frac{2}{\pi}\langle\cos 2z\;\partial_z\left[\sin z\;C_1(z)\right]\rangle = 0.658, \quad I_2 = \frac{2}{\pi}\langle\cos z\;C_1(z)\rangle = 0.787. \tag{6.19}$$

Again, the expressions for the stationary regime are obtained by substituting $\tilde{\omega}^2 \to \lambda_\sigma^2$ and $\omega_H \to 0$ in the Eqs (6.15) - (6.18).

Both excited modes are pure charge-carrier modes. The mode $\boldsymbol{u}_0^{(2)}$ is homogeneous in x, so the corresponding effective viscosity $\hat{\eta}^{(\mathrm{eff})}$ [Eq. (5.28) for $q = 0$ and appropriate projection integrals] diverges. This leads in Eq. (6.13) for very small q to $\hat{C}^2/\hat{\sigma}_a^{(\mathrm{eff})} = \epsilon_\perp \alpha_3 q^2/(\sigma_\perp \eta_2)$ times some projection integrals, i.e., the coupling of σ to n_z vanishes for $q = 0$. The σ part of $\boldsymbol{u}_2^{(2)}$ does not excite the director either, because this mode has no z dependence and the couplings are $\propto \partial_z \sigma$ and $\partial_z n_z$. The inhomogeneity (6.14) excites further modes, e.g., a mode with $(\sigma, n_z) \propto (\cos 2z, n_2 \sin 2z) e^{2i(\mathbf{q}_c \cdot \mathbf{x} + \omega_H t)}$. These modes, however, relax faster and the couplings have smaller projection integrals; they will be neglected.

At order $\epsilon^{3/2}$, the inhomogeneous system for $\sigma^{(3)}$ and $n_z^{(3)}$ reads

$$\underline{\underline{\tilde{L}}} \begin{pmatrix} \sigma^{(3)} \\ n_z^{(3)} \end{pmatrix} \equiv \boldsymbol{I}^{(3)} = - \begin{pmatrix} \boldsymbol{v}^{(1)} \cdot \boldsymbol{\nabla} \sigma^{(2)} + R_c \tilde{\alpha}^2 \sigma_a^{(\mathrm{eff})} \, g^{\mathrm{SM}} |A|^2 \partial_x \partial_z n_z^{(1)} \\ g^{\mathrm{SM}} |A|^2 \left(\frac{\partial_x n_z^{(1)}}{\tau_0^{\mathrm{SM}}} + \frac{R_c C^2}{\sigma_a^{(\mathrm{eff})}} \partial_z \sigma^{(1)} \right) \end{pmatrix}. \tag{6.20}$$

where $\underline{\underline{\tilde{L}}}$ denotes the matrix-differential operator on the left-hand sides of the Eqs. (6.4) and (6.5). The advection term of the excited charge-carrier density is given (within the lowest-order Galerkin expansion) by

$$\boldsymbol{v}^{(1)} \cdot \boldsymbol{\nabla} \sigma^{(2)} = \frac{1}{2} R_c \tilde{\alpha}^2 \sigma_a^{(\mathrm{eff})} \, \gamma_\sigma i q_c |A|^2 A \sin z e^{i(\mathbf{q}_c \cdot \mathbf{x} + \omega_H t)} + \text{c.c.} + \text{nonresonant terms}, \tag{6.21}$$

where γ_σ describes, both for the Hopf ($\tilde{\omega}^2 = \omega_H^2 + \lambda_\sigma^2$) and stationary ($\omega_H \to 0$) regimes, the nonlinearities originating from the σ modes,

$$\gamma_\sigma = \frac{|\lambda_\sigma|}{(\omega_H^2 + \lambda_\sigma^2)(\tau_0^{\mathrm{SM}})^2} \left(\frac{I_0^2}{\lambda_0^{(2)}} + \frac{I_2^2 (1 + \frac{i\omega_H}{\lambda_\sigma})}{\lambda_2^{(2)}} \right) g_\sigma, \tag{6.22}$$

$$g_\sigma = \frac{\pi}{4} \left(\frac{K^{(\mathrm{eff})} \, \tau_0^{\mathrm{SM}}}{q_c} \right)^2. \tag{6.23}$$

Note, that the prefactor $|\lambda_\sigma|/[\tau_0^{\mathrm{SM}}(\omega_H^2 + \lambda_\sigma^2)]$ can be written as $\Delta\epsilon/(\tilde{\omega}\tau_0^{\mathrm{SM}})^2$ for both regimes where the threshold shift $\Delta\epsilon$ is given by Eq. (5.50).

Since the inhomogeneity $\boldsymbol{I}^{(3)}$ in Eq. (6.20) has "resonant" terms in the kernel of the adjoint linear operator, there is a nontrivial solvability condition yielding the Landau equation $\partial_t A = \epsilon A - g(1 + ic)|A|^2 A$, whose nonlinear terms are also that of the CGL (6.3). The canonical procedure consists in projecting $\boldsymbol{I}^{(3)}$ onto the eigenvector of the adjoint linear problem with the eigenvalue λ^*. Here I present a more intuitive approach stressing the concept of the amplitude-dependent effective coefficients that is equivalent.

Substituting in Eq. (6.20) the fields $(\sigma^{(1)}, n_z^{(1)}) = e^{i\mathbf{q}_c\cdot\mathbf{x}}(\overline{\sigma}, \overline{n}_z)$ where $\overline{\sigma}$ and $\overline{n}_z$ are given by the Galerkin approximations (5.40) and (5.39), projecting separately the upper line of Eq. (6.20) onto $(2/\pi)^{1/2}\sin z$ and the lower line onto $(2/\pi)^{1/2}\cos z$, [6] and adding the nonresonant linear terms, gives a quasi-linear generalization of the 2×2 system (5.38),

$$\begin{array}{rrl} (\partial_t - \lambda_\sigma)\, A_\sigma(t) & +R\tilde{\alpha}^2\sigma_a^{(\mathrm{eff})}\ (1 - (\gamma_\sigma + g^{\mathrm{SM}})|A|^2)\, A_n(t) & = 0, \\ -\frac{RC^2}{\sigma_a^{(\mathrm{eff})}}\,(1 - g^{\mathrm{SM}}|A|^2)\, A_\sigma(t) & + \left(\partial_t - \lambda_n + \frac{g^{\mathrm{SM}}}{\tau_0^{\mathrm{SM}}}|A|^2\right) A_n(t) & = 0, \end{array} \tag{6.24}$$

where A_n is related to the CGL amplitude by

$$A_n(t) = \bar{A}_{\mathbf{q}-\mathbf{q}_c}(t)e^{i\omega(\mathbf{q}_c,\epsilon)t}. \tag{6.25}$$

The determinantal condition of Eq. (6.24) gives, as generalization of Eq. (5.47), the amplitude-dependent growth rate λ_{NL}

$$\begin{aligned} \lambda_{\mathrm{NL}} &= \frac{\lambda_\sigma + \tilde{\lambda}_n}{2}\ \overset{+}{(-)}\ \sqrt{\frac{(\tilde{\lambda}_n - \lambda_\sigma)^2}{4} - \tilde{\omega}^2\,(1 - (\gamma_\sigma + 2g^{\mathrm{SM}})|A|^2)} \\ &+ \mathcal{O}(|A|^4), \end{aligned} \tag{6.26}$$

$$\tilde{\lambda}_n = \lambda_n - \frac{g^{\mathrm{SM}}|A|^2}{\tau_0^{\mathrm{SM}}}. \tag{6.27}$$

In analogy to the linear case, the amplitude equation is given, to order $\epsilon^{3/2}$, by Eq. (6.7) with the Taylor expansion of λ replaced by that of λ_{NL} around $\boldsymbol{q} = \boldsymbol{q}_c, \epsilon = 0$ and $|A|^2 = 0$.

Comparing the Taylor expansion with Eq. (6.3) leads to the nonlinear contributions

$$g(1 + ic) = -\tau_0 \frac{\partial \lambda_{\mathrm{NL}}}{\partial |A|^2}. \tag{6.28}$$

Evaluating Eq. (6.28) with the Eqs. (6.26), (6.22), (6.23), (6.18), and (6.19) finally gives the nonlinear CGL coefficients, summarized in Table 6.2.

The Figures 6.1c, 6.1d, and 6.2d give, for I 52 parameters, plots of these expressions as functions of $\tilde{\alpha}$ and $\tilde{r}$. The chosen $\tilde{\alpha}$ and $\tilde{r}$ values are in the experimentally relevant range (for 28 μm cells of I 52, values of $\tilde{\alpha}$ consistent with the measured Hopf frequency vary from $\tilde{\alpha} = 0.011$ at 60°C to $\tilde{\alpha} = 0.038$ at 30°C).

Remarkabally, the saturation coefficient g^{stat} in the stationary regime is negative near the C2 curve indicating a hysteretic bifurcation. Intuitively, the advection "washes away" the σ fields thus decreasing the threshold shift connected with them. For increasing $\tilde{r}$, the σ field cannot build up to amplitudes causing a significant

[6] This is just the lowest-order Galerkin approximation of the system (6.20).

Table 6.2: Nonlinear coefficients of the complex Ginzburg–Landau equation (6.3)

Regime	Coefficient	Expression for $R_c\tilde{\alpha}^2 << 1$
Hopf	g	$g^{\mathrm{SM}} + \frac{(\tilde{r}+2\lvert\lambda_\sigma\rvert)I_2^2}{\tau_0^{\mathrm{SM}}(\tilde{r}^2+4\omega_H^2)} g_\sigma$
	gc	$\frac{\lvert\lambda_\sigma\rvert}{\omega_H \tau_0^{\mathrm{SM}}} \left[\frac{I_0^2}{\tilde{r}+4R_c\tilde{\alpha}^2} + \frac{I_2^2\left(\tilde{r}+\frac{2\omega_H^2}{\lambda_\sigma}\right)}{\tilde{r}^2+4\omega_H^2} \right] g_\sigma + \left[\frac{2\tau_0^{\mathrm{SM}}\tilde{\omega}^2}{\omega_H} - \frac{\lvert\lambda_\sigma\rvert}{\omega_H} \right] g^{\mathrm{SM}}$
Stationary	g^{stat}	$\left(1 - \frac{2\tau_0^{\mathrm{SM}}\tilde{\omega}^2}{\lvert\lambda_\sigma\rvert}\right) g^{\mathrm{SM}} - \frac{\tilde{\omega}^2}{\tau_0^{\mathrm{SM}}\lambda_\sigma^2} \left(\frac{I_0^2}{\tilde{r}+4R_c\tilde{\alpha}^2} + \frac{I_2^2}{\tilde{r}} \right) g_\sigma$

threshold shift, and eventually, the bifurcation becomes forward. For increasing $\tilde{\alpha}$, the drift velocity of the charge carriers increases with respect to the fluid velocity at a given ϵ, so that the advection effects get weaker causing an increasing g^{stat} at points with a constant distance $\tilde{r} - \tilde{r}_{\mathrm{C2}}$ from the C2 point. This is true especially at the stationary side of the C2 curve itself, shown in Fig. 6.1d.

On the Hopf side, the saturation is *stronger* than in the SM ($g > g^{\mathrm{SM}}$), and the frequency decreases with increasing amplitude ($b > 0$), unless the recombination rate is very small. The frequency decrease can be made plausible with the help of the nonlinear growth rate (6.26). For not too high $\tilde{\alpha}$, the term $\propto \gamma_\sigma |A|^2$ in Eq. (6.26) dominates. The real part of γ_σ describes the decrease of the $\sigma - n_z$ coupling and leads to a decrease of the oscillation frequency, in analogy to decreasing the oscillation frequency of a spring by decreasing the spring constant.

6.3 Comparison with experimental results

In this Section, I compare the weakly-nonlinear results of Chapter 6.2 with experiments on I 52 [42, 30, 31] and with some results of the the group of Rehberg on MBBA [39, 44, 41, 40].

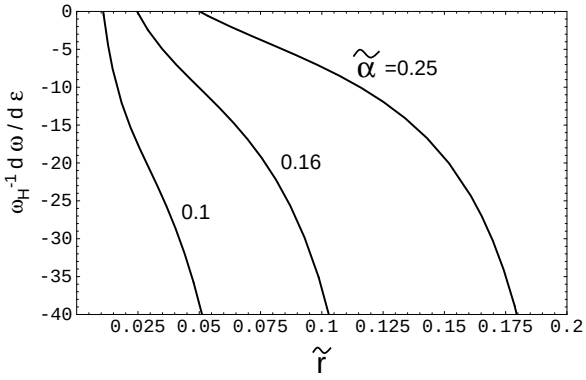

Figure 6.3 Frequency decrease $\frac{1}{\omega_H}\frac{d\omega}{d\epsilon} := -\Delta^{-1}$ due to the linear and nonlinear frequency shifts, calculated from Eq. (6.29) as function of $\tilde{\alpha}$ and $\tilde{r}$ for I 52 parameters. The value $\tilde{\alpha} = 0.16$ corresponds to $T = 49°$C where the frequency decrease was measured.

6.3.1 Decrease of the oscillation frequency with the control parameter

On increasing the control parameter above its threshold value in the Hopf regime, a decrease of the frequency of the travelling rolls was measured. In MBBA, the decrease, in units of the Hopf frequency, was $\Delta^{-1} := -\frac{1}{\omega_H}\frac{d\omega_H}{d\epsilon}|_c \approx 2.1$ for a 15 μm cell at $\omega_0\tau_q = 1.1$ [41] and ≈ 15 in Ref. [40]. In I 52, $\Delta^{-1} \approx 11$ for a 28 μm cell at $\omega_0\tau_q = 1.34$ and 49°C [31] was measured. Note that Δ defines the control parameter ϵ at which a linear extrapolation of the frequency decrease would lead to stationary patterns.

The theoretical dependence of ω on the control parameter is composed of the linear and the nonlinear frequency shifts, $\frac{d\omega}{d\epsilon} = \frac{\partial\omega}{\partial\epsilon} + \frac{\partial\omega}{\partial|A|^2}\frac{\partial|A|^2}{\partial\epsilon}$, where $\frac{\partial\omega}{\partial|A|^2} = -gc/\tau_0$. For stationary conditions (not to be confused with the stationary regime), the amplitude of the critical mode is $|A|^2 = \epsilon/g^{\mathrm{stat}}$ leading to the theoretical prediction

$$\frac{d\omega}{d\epsilon} = \frac{\partial\omega}{\partial\epsilon} - \frac{c}{\tau_0}, \tag{6.29}$$

whith $\frac{\partial\omega}{\partial\epsilon}$ and c from the Tables 6.1 and 6.2.

Fig 6.3 shows that the frequency decrease depends rather strongly on $\tilde{r}$. The experimental value of $\Delta^{-1} = 11$ in the I 52 experiments ($\tilde{\alpha} = 0.016$) is consistent with $\tilde{r} = 0.045$ corresponding to a recombination time of about 10 sec. This has to be compared with the result $\tau_{\mathrm{rec}} = 20$s obtained from the C2 point in Chapter 5. While this factor of two can be attributed to the approximations (e.g., $\omega_0\tau_q << 1$) made in calculating the nonlinear CGL coefficient b, further work is needed to clarify if the strong dependence of Δ^{-1} and c on $\tilde{r}$ is an artefact of the approximations. In particular, c gets negative for very small recombination rates which is rather unsure.

Generally, the magnitude of the change of the relative oscillation frequency decreases with increasing $\tilde{\alpha}$, in qualitatve agreement with the lower value for MBBA corresponding to $\tilde{\alpha} = 0.025$.

6.3.2 Phase diagrams

The figures 6.4 and 6.5 show, for I 52 parameters and for $\omega\tau_q << 1$, the typical weakly-nonlinear regimes in the $(\tilde{\alpha}, \tilde{r})$ space, predicted by the WEM. The codimension-two curve $|\lambda_\sigma| = \tilde{\omega}$ separating the Hopf regime from the stationary regime (labelled with "C2") derives already from the linear considerations in Chapter 5.4. With the Eqs. (5.41) and (5.48), the condition for a Hopf bifurcation can be formulated as $\tilde{r} < R_c\tilde{\alpha}(C - \tilde{\alpha}\epsilon_q/\sigma_q)/(1+\omega'^2)$, i.e., there is always a Hopf bifurcation for sufficiently small reombination rates, apart from extreme values of $\tilde{\alpha}$.

Neighbouring the C2 curve on the stationary side is a region where the bifurcation is hysteretic. Further away from the C2 curve, the bifurcation gets forward at the tricritical curve "TC", and, in the limit $\tilde{r} \to \infty$, the asymptotic dynamics is that of the SM. For small $\tilde{\alpha}$, the tricritical curve is approximately given by $\tilde{r}_{\rm tri} = [g_\sigma(I_0^2 + I_2^2)/(\tau_0^{\rm SM} g^{\rm SM})]^{1/3}\tilde{\omega}^{2/3}$. For a higher SM saturation $g^{\rm SM}$ or a lower g_σ (increasing $g^{\rm SM}/g_\sigma$ by a factor of four, or more), the TC curve would cross the C2 curve. In this case, there exists a range of values for $\tilde{\alpha}$ where the bifurcation is forward for all values of $\tilde{r}$.

In contrast to the SM parameters entering most aspects of the dynamics in the conductive regime only as relative quantities ($\sigma_a/\sigma_\perp$, etc.), the WEM parameters $\tilde{\alpha}$ and $\tilde{r}$, defined in Table 3.4, depend on the thickness d and on the absolute values of the SM parameters which are changed by the temperature as a "third control parameter" besides R and ω_0. Varying the temperature and using different cells, a representative part of the phase diagram is accessible with only one type of NLC. The mobility parameter $\tilde{\alpha} \propto (\gamma_1/\sigma_\perp)^{1/2} d^{-1}$ can be increased by choosing lower temperatures (increasing γ_1, decreasing $\sigma_\perp$) or by a thinner cell; by contrast, the recombination parameter $\tilde{r} \propto \gamma_1 d^2/(K_{11}\tau_{\rm rec})$ decreases by choosing a thinner cell. Presumably, $\tilde{r}$ increases with temperature, for example, by an activation-energy like behaviour of the equilibrium ion density $n_0 \propto \tilde{r} \propto 1/\tau_{\rm rec}$ (Table 3.4).

The cross in the upper left corner of Fig. 6.4 indicates the point in parameter space corresponding, for an assumed recombination rate of 20 s, to $d = 28$ μm and 30°C. The thick arrow pointing to the stationary-hysteretic region shows the change in $(\tilde{\alpha}, \tilde{r})$ space expected when going to a 56 μm cell at the same temperature. The experimentally observed bifurcation for such cells is, indeed, stationary, but this has been used in Chapter 5.5.2 to determine the recombination time. Independent from the recombination time, however, is the fact that the stationary bifurcation is hysteretic near the C2 point and that the Hopf bifurcation is always continuous. [7]

The dotted arrow shows the change in $(\tilde{\alpha}, \tilde{r})$ space caused by heating the 28 μm I 52 cell to 60°C under the (questionable) assumption of a constant recombination time of 20 s. If the recombination time decreased with temperature, e.g., in parallel

[7] There exist measurements on MBBA which have been interpreted as a hysteretic Hopf bifurcation [39]. They will discussed in Chapter 6.3.3.

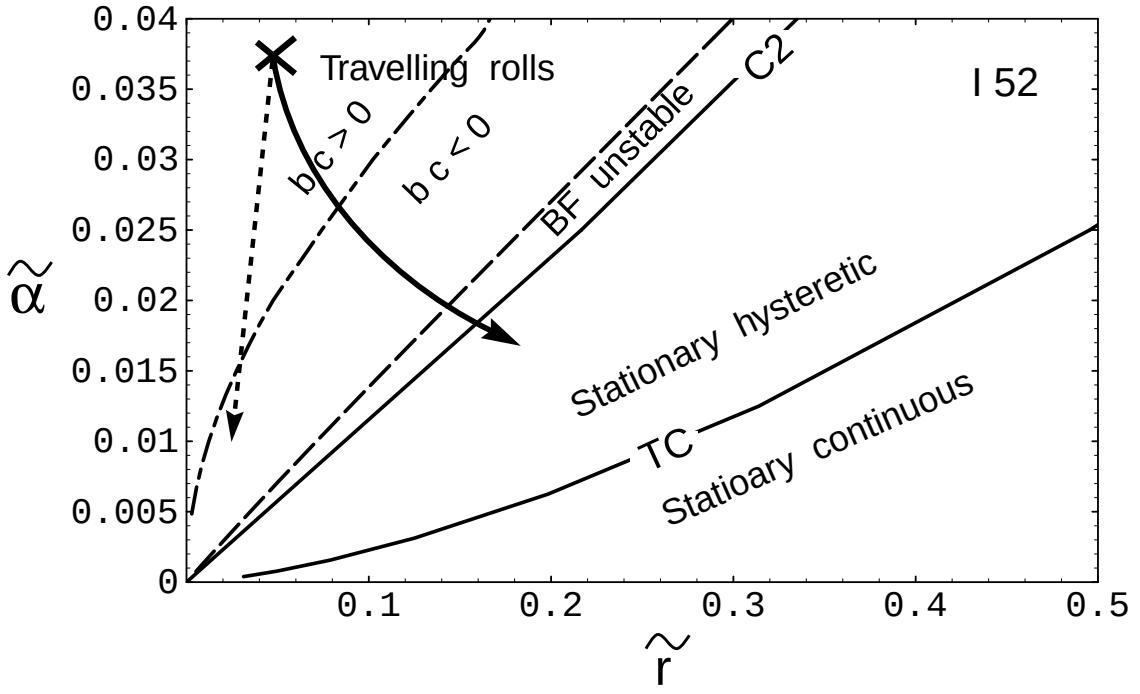

Figure 6.4 Phase diagram of the weakly-nonlinear behaviour in the parameter space $(\tilde{\alpha}, \tilde{r})$ for I 52 parameters at 45°C, and for external frequencies satisfying $\omega_0 \tau_q << 1$. The curve labelled with C2 is the codimension-two curve $|\lambda_\sigma| = \tilde{\omega}$ separating the Hopf regime of travelling waves from the stationary regime. At the stationary side, the bifurcation is hysteretic in a rather large region bounded by the C2 curve and the tricritical curve labelled "TC". For large $\tilde{r}$ or low $\tilde{\alpha}$, the bifurcation becomes continuous and, in the limit $\tilde{r} \to \infty$, the SM behaviour is recovered. In the Hopf regime, the product bc of the dispersion coefficient and of nonlinear frequency shift is positive for very small recombination rates $\tilde{r}$ Approaching the C2 curve it becomes negative at the dashed-pointed curve and in the neighbourhood of the C2 curve there is a small "baloon" bounded by the dashed curves, where the one-dimensional Benjamin-Feir criterion $bc < -1$ is fulfilled.

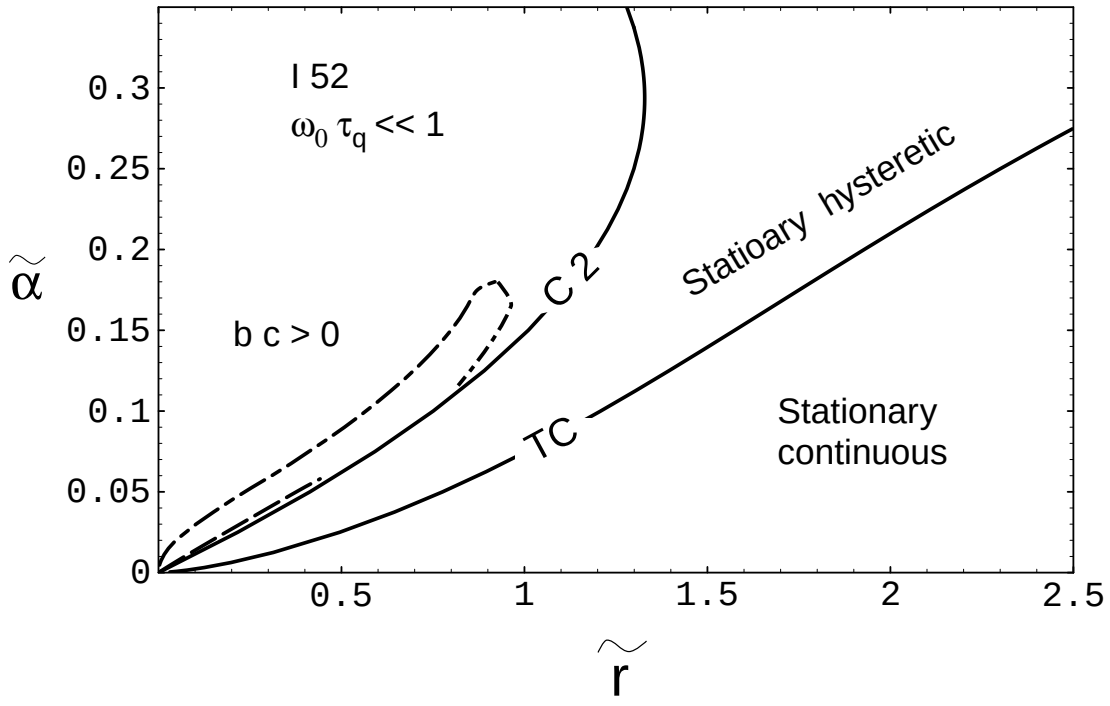

Figure 6.5 Phase diagram for the same parameters as in Figure 6.4, but for larger values of $\tilde{\alpha}$ and $\tilde{r}$, relevant for thinner cells and/or higher recombination rates. The bending of the C2 curve is due to the $\tilde{\alpha}^2$ term in the growth rate of the σ mode, Eq. (5.41). Above $\tilde{\alpha} = 0.018$, there are severeal $\tilde{r}$ values where the product bc changes the sign, but where, in general, $|bc| << 1$.

with the director relaxation time (both times are related to activation-energy processes), the arrow would point more to the right. For $\tau_{\rm rec} < 5s$, one would obtain a stationary bifurcation at T>60°C, in accordance with some measurements [30, 31]. There are, however, some intricacies connected with this observation which will be discussed in the next Chapter 6.3.3.

There is a very thin tongue in the Hopf regime (dashed lines in the Figures 6.4 and 6.5) where the one-dimensional Benjamin–Feir (BF) criterion $bc < -1$ is fulfilled. Within the one-dimensional CGL, all plane-wave solutions are unstable against long-wavelength modulations in this region, resulting in spatiotemporal chaos (STC) [11] for the envelope of the travelling waves. Experimentally, one found in I 52 at $T > 50$°C a Hopf bifurcation to STC. [8] At these temperatures, one is, indeed, nearer to the BF unstable region than for lower temperatures or crosses even the BF unstable region (arrow with the dashed line in Fig. 6.4), but the range, where STC is observed, is much broader than this region. The one-dimensional BF condition, however, is only a *sufficient* criterion for STC if there is more than one spatial dimension or if couplings to other critical modes are relevant. For instances, if the coupling (which has yet to be investigated) is such that a small change in the coupling coefficients leads to a nonlinear selection of a different mode configuration (e.g., oblique rolls *vs* square patterns if the roll angle is not too different from 45 degrees), the BF criterion for STC gets weaker with the extreme case $bc < 0$ [110]. In the Figures 6.4 and 6.5, the larger region where $bc < 0$ is bounded by the dashed lines and by the immediate neighbourhood of the C2 curve (not resolved on the plots). It corresponds semiquantitatively to the parameter ranges where STC is observed in I 52.

6.3.3 Hysteretic effects

Stationary regime

In the I 52 experiments, stationary bifurcations were always hysteretic, in accordance with the WEM predictions not too far away from the C2 curve. The amplitude (maximum director angle) of the nonlinear state right after the jump was found to be 200 mrad ($|A_{\rm NL}| = 0.2$) in a 57 μm cell at 47°C [31].

Strictly speaking, with a third-order CGL like Eq. (6.3), nothing more can be said about hysteretic effects beyond the fact that the bifurcation *is* hysteretic or not. Some properties specific to the WEM, however, enable some predictions on this level. The effects of the σ fields always stabilize the system, so an upper limit of the amplitude $|A_{\rm NL}|$ of the nonlinear state after the hysteretic jump is set by the SM amplitude. Moreover, both the excitation and the relaxation of the σ fields take place on long time scales. This translates to small hysteretic jumps to nonlinear amplitudes

[8] At lower temperatures, one observed localized (and also irregular) states.

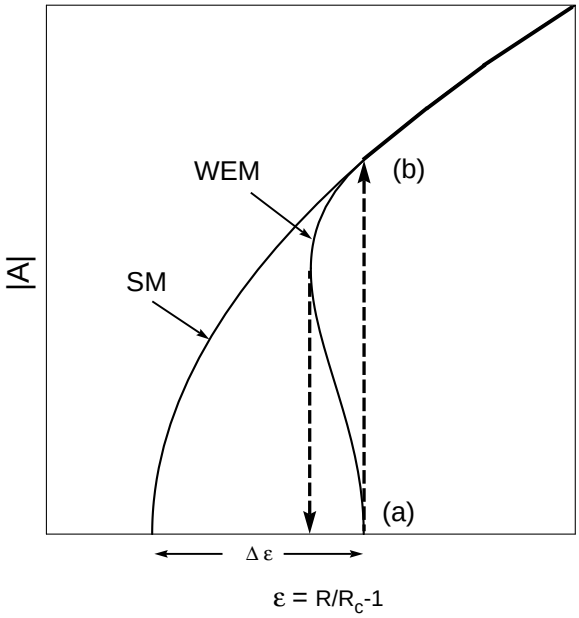

Figure 6.6 Schematic illustration of a hysteretic bifurcation from the linear WEM state (a) to a nonlinear state (b). $\Delta\epsilon$ denotes the linear threshold shift separating the neutral-stability curves of the SM and the WEM at threshold. Shown is a situation where, at the point (b), the SM and WEM amplitudes are not distinguishabel, i.e., the σ fields have no influence on the nonlinear state.

where, presumably, the amplitude equation of the SM is still valid. At last, if the condition for a hysteretic bifurcation is well satisfied by, say, $g^{\rm stat}_{\rm WEM}/g^{\rm SM} < -1$ (one is not too near the TC curve), it is plausible that the advection homogenizes the carrier density in the nonlinear state so that this state is presumably described by the SM.

With these assumptions, it can be seen from Fig. 6.6, that the amplitude in the nonlinear state (b) is that of the weakly-nonlinear SM with $\epsilon^{\rm SM} = R/R_c^{\rm SM} - 1$ equal to the linear threshold shift,

$$|A_{\rm NL}|^2_{\rm stat} = \frac{\Delta\epsilon}{g^{\rm SM}} = \frac{\tilde{\omega}^2\tau_0^{\rm SM}}{|\lambda_\sigma| g^{\rm SM}}. \tag{6.30}$$

The highest jump takes place on the (stationary side of) the C2 curve with $A_{\rm NL}|^2_{\rm stat} \approx \tau_0^{\rm SM}/(g^{\rm SM}\tau_{\rm rec})$.

The experimental parameters used for the hysteresis measurements in I 52 correspond to a point near the C2 curve. This can be seen from Fig. 5.10 where the lower curve is for a cell of a comparable thickness at a comparable temperature. With $\tau_0^{\rm SM} = 0.33$ s and $\tau_{\rm rec} = 20$ s, Eq. (6.30) gives at the C2 point the theoretical result $|A_{\rm NL}| = 0.184$.

Hopf regime

The WEM always predicts a continuous bifurcation in the Hopf regime. Indeed, one observes in I 52, that the initial bifurcation to oscillating states is continuous. At

a rather small value $\epsilon_{\rm jp}$, however, the travelling-wave state with the amplitude $|A_{\rm jp}|$ and the finite oscillation frequency $\omega_{\rm jp} < \omega_H$ jumps hysteretically to a stationary state with a much higher amlitude $|A_{\rm NL}|$ (see Fig. 6.7). For $d = 28$ μm , $\epsilon_{\rm jp}$ varied from 0.1 at 44°C to 0.02 at 59°C [31]. At even higher temperatures, a *hysteretic* stationary bifurcation was observed as primary bifurcation. Due to the large steps of the reduced control parameter ($\delta\epsilon \approx 0.01$) in this experiment, it could not be excluded, however, that the initial bifurcation is actually a *continuous Hopf* bifurcation with a subsequent jump to a nonlinear stationary state at a very small $\epsilon_{\rm jp}$ which could not be resolved.

In MBBA, the bifurcations appeared continuous in experiments without excessive sensitivity in optical contrast and resolution in ϵ [41, 111, 112]. In other very careful investigations, primarily devoted to thermal fluctuations below threshold and discussed in Chapter 7 [44, 39], one observed hysteretic bifurcations to a nonlinear stationary state. The amplitude was about 150 mrad in the experiment of Ref. [39]. The spatiotemporal correlations of *sub-threshold* fluctuations in the same cells, however, can be explained only by assuming a Hopf bifurcation for the linear dynamics, with a very small Hopf frequency of $\omega_H/(2\pi) = 0.044$ s in Ref. [39] and 0.05 s in Ref. [44] (see Chapter 7 for more details). Can this "hysteretic Hopf bifurcation" be explained by assuming, again, a continuous Hopf bifurcation in a regime $0 < \epsilon < \epsilon_{\rm jp}$ which cannot be resolved experimentally?

To describe the dynamics of this scenario with Ginzburg–Landau equations seems hopeless. One needed a seventh-order (!) CGL, and the amplitudes where the higher-order terms come into play, would be higher than the range were a CGL description is even *qualitatively* correct. By contrast, a semi-quantitative description seems possible for the hysteresis by exploiting the quasi-linear 2×2 equations (6.24) and assuming, again, that the amplitude of the nonlinear state is given by the amplitude equation of the SM.

From the determinantal condition of the system (6.24) for zero growth, $\lambda = i\omega$, one obtains, neglecting terms $\propto |A|^4$,

$$-\omega^2 + \frac{\lambda_\sigma}{\tau_0^{\rm SM}}(\epsilon^{\rm SM} - g^{\rm SM}|A|^2) + \tilde{\omega}^2\left(1 - ({\rm Re}\gamma_\sigma + 2g^{\rm SM})|A|^2\right) = 0, \qquad (6.31)$$

$$\omega\left(\lambda_\sigma + \frac{\epsilon^{\rm SM} - g^{\rm SM}|A|^2}{\tau_0^{\rm SM}}\right) - \tilde{\omega}^2 {\rm Im}\gamma_\sigma |A|^2 = 0, \qquad (6.32)$$

where γ_σ is given by Eq. (6.22) with ω_H replaced by the actual oscillation frequency ω. The roots of the system (6.31), (6.32) determine the generalized neutral curves. For the oscillatory branch, the result is (Note that $\epsilon^{\rm SM} = \epsilon + |\lambda_\sigma|\tau_0^{\rm SM}$)

$$\epsilon_{\rm osc} = g(\omega)|A|^2, \qquad (6.33)$$

$$\omega^2 = \omega_H^2 - \frac{|\lambda_\sigma| g(\omega)}{\tau_0^{\rm SM}}\left(1 + \frac{\omega c(\omega)}{|\lambda_\sigma|}\right)|A|^2, \qquad (6.34)$$

where $g(\omega)$ and $c(\omega)$ are the nonlinear CGL coefficients in Table 6.2 with ω_H replaced by ω. For the stationary branch $\omega = 0$ one obtains

$$\epsilon^{\rm stat} = \Delta\epsilon^{\rm stat} + g^{\rm stat}|A|^2, \qquad \Delta\epsilon^{\rm stat} = \frac{\tau_0^{\rm SM}\omega_H^2}{|\lambda_\sigma|}. \tag{6.35}$$

Figure 6.7 illustrates schematically the resulting hysteresis curves. For small amplitudes, the oscillatory branch has the lowest threshold. On increasing ϵ, the amplitude is given initially by $|A|^2 = \epsilon/g$ and the frequency decreases initially with the rate $\frac{d\omega}{d\epsilon}$, Eq. (6.29). The bending of the amplitude curve is due to the frequency dependence of $g(\omega)$. With $g(\omega) > g > g^{\rm SM}$, this branch has comparatively small amplitudes. The stationary branch is the same as in the stationary regime; it is extremely hysteretic since $g^{\rm stat}$ (Table 6.2) becomes more negative for decreasing $\tilde{r}$ (the dashed curves in Figure 6.1c have to be extrapolated to $\tilde{r} < |\lambda_\sigma|$).

Because of the frequency mismatch, the system cannot cross over from the oscillatory curve to the stationary curve at the point B in Fig. 6.7. The actual point where the jump takes place, has not yet been determined, so the points C and D in Figure 6.7 are qualitative and based on experiments where the jump takes place at an oscillation frequency of about half the Hopf frequency [31].

For very small Hopf frequencies as in Ref. [39], an upper bound can be given for the control parameter at the hysteretic jump $\epsilon_{\rm jp}$ (see Figure 6.7), $\epsilon_{\rm jp} \approx \Delta/2 \propto (\tilde{\omega}\tau_0^{\rm SM})^2$. $\epsilon_{\rm jp}$ decreases strongly with $\tilde{r}$. For $\tilde{r} = 0.5\tilde{\omega}$, it is smaller than the step size $\delta\epsilon = 0.001$ of the experiment so that a forward Hopf bifurcation may go unnoticed. Besides, the amplitude $|A|^2_{\rm jp} = \epsilon_{\rm jp}/g \approx 13$ mrad at the jump is very small; it is only three times larger than typical rms values in the subcritical regime of (thermal) fluctuations (!). This is caused by the combined effects of a small value of $\epsilon_{\rm jp}$, and a high saturation coefficient, $g/g^{\rm SM} = 6.5$ for $\tilde{r} = 0.5\tilde{\omega}$. In contrast, the nonlinear amplitude $|A_{\rm NL}|^2 = (\epsilon_{\rm jp} + \Delta\epsilon)/g^{\rm SM} \approx 100$ mrad increases with $\tilde{r}$, caused by the increased linear threshold shift.

6.4 Discussion

The weakly-nonlinear analysis of the WEM agrees qualitatively and sometimes quantitatively with the experiments. At first, the calculation of the CGL coefficients brought two linear results. The correlation time τ_0 in the Hopf regime is twice that of the SM while the correlation length is the same in both models. Both results fit well to experimental values obtained for cells of 13 μm [39] and 23 μm [44] thickness from the oscillating dynamics in the subcritical stochastic regime. There seem to be no measurements of τ_0 in I 52.

The phase diagram of the weakly-nonlinear behaviour agrees qualitatively. In particular, the Hopf bifurcations are always continuous and the stationary bifurcations

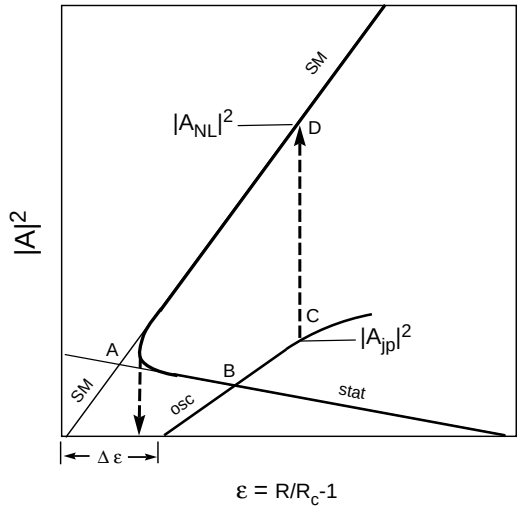

Figure 6.7 Hysteretic secondary bifurcation in the Hopf regime (schematically). The curve labelled "stat" is the stationary backwards-bifurcating branch of zero growth rate which exists also in the stationary regime. At the point A (where the amplitude is of the order of $|A| \approx |\lambda_\sigma|$), the stationary branch crosses over to the SM branch "SM". The curve labelled "osc" is the oscillatory branch starting with the Hopf frequency. The oscillation frequency decreases with ϵ until the curve ends at zero frequency. At the point C, the state jumps from the continuous Hopf branch to the nonlinear SM state D.

are hysteretic if one is near the C2 curve. The observed STC for higher temperatures in I 52 is compatible with the area in phase space where the WEM predicts $bc < 0$. This can possibly be explained by a Benjamin–Feir like long-wavelength instability.

Both, linear and nonlinear results for I 52, are compatible with a recombination time of 10 to 20 s. The decrease of the oscillation frequency of travelling waves with the control parameter is compatible with $\tau_{\rm rec} = 10$ s. The amplitude of the nonlinear state in the stationary-hysteretic regime requires $\tau_{\rm rec} \approx 15$ s. Comparing the C2 curve with the external parameters (cell thickness, temperature, ω_0) where the Hopf frequency decreases to zero, gives $\tau_{\rm rec} \approx 20$ s. In MBBA, the condition $|\lambda_\sigma| < \tilde{\omega}$ required $\tau_{\rm rec} > 1/\omega_H = 3.5$ s in the experiment of Ref. [39].

The oscillatory behaviour observed for MBBA in the subcritical stochastic regime, while a hysteretic jump to stationary patterns is observed above threshold [39], seems puzzling. Even this seems to be consistent with the WEM assuming a continuous Hopf bifurcation, but a jump to a stationary state at a small but positive control parameter $\epsilon_{\rm jp}$ which cannot be resolved experimentally. For typical experimental resolutions $\delta\epsilon < 0.001$, this implies $\tilde{r} \geq 0.4$ or $\tau_{\rm rec} \leq 8$ s. The reason for the small $\epsilon_{\rm jp}$ is the small Hopf frequency where Eq. (6.29) together with the CGL coefficient c in Table 6.2 lead to $\epsilon_{\rm jp} \approx \Delta/2 \propto (\tilde{\omega}\tau_0^{\rm SM})^2$. Recent experiments on the nematic mixture Merck Phase 5 confirm this interpretation [113].

An interesting prediction of the theory is that the nonlinear dispersion c becomes negative for very small recombination rates, i.e., the oscillation frequency should increase with the amplitude (the linear frequency shift can be neglected for small $\tilde{r}$), which has never been observed. Possibly this is due to the dynamics of the excited charge-carrier modes which become dynamically independent for small recombination rates so that the CGL is valid only in a very small range of ϵ. The CGL requires that all excited modes relax much faster than the amplitude itself, $\tau_0^{-1}\epsilon << |\lambda_0^{(2)}|$, $|\lambda_2^{(2)}|$, or

$$\epsilon << \tau_0\tilde{r} \approx 2\Delta\epsilon. \tag{6.36}$$

The CGL of the WEM is valid, if the distance from threshold is much smaller than the linear threshold shift. For I 52, this gives $\epsilon << 0.02$ (Table 6.3), and in MBBA, e.g., $\epsilon << 0.01$ for the cell in Table 6.3 assuming $\tilde{r} = 0.5\tilde{\omega}$. With a typical resolution of $\delta\epsilon = 10^{-3}$, this range is experimentally accessible.